Available online at www.sciencedirect.com

ScienceDirect

Procedia Structural Integrity 5 (2017) 697–704

Structural Integrity Procedia

www.elsevier.com/locate/procedia

2nd International Conference on Structural Integrity, ICSI 2017, 4-7 September 2017, Funchal, Madeira, Portugal

Effect of rivet holes on calibration curves for edge cracks under various loading types in steel bridge structure

Stanislav SEITL[a]*, Petr MIARKA[a,b], Zdeněk KALA[b], Jan KLUSÁK[a]

[a]*Institute of Physics of Materials, Academy of Sciences of the Czech Republic, Zizkova 22, 616 62, Czech Republic*
[b]*Faculty of Civil Engineering, Brno University of Technology, Veveří 331/95, Brno 602 00, Czech Republic*

Abstract

Attention has been paid to fatigue cracks in steel structures and bridges for a long time. In spite of efforts to eliminate the creation and propagation of fatigue cracks throughout the designed service life, cracks are still revealed during inspections. There is some limitation of crack sizes which are detectable on structure (from 2 up to 10 mm). Note that depending on the location of the initial crack, the crack may dominantly propagate from the edge or from the surface. The theoretical model of fatigue crack progress is based on linear elastic fracture mechanics. Steel specimens are subjected to various load types (tension, three- and four-point bending, pure bending etc.). The calibration functions for short edge cracks that are near the hole for a rivet or bolt are compared for various loads and the discrepancies are discussed.

Peer-review under responsibility of the Scientific Committee of ICSI 2017

Keywords: edge cracks; rivet holes; fracture mechanics; calibration curves; stress intensity factor;

1. Introduction

The residual life prediction of old riveted steel bridges will be a relatively difficult task. Riveting is no longer common practice, consequently finding good equipment and skilled riveters is difficult (see e.g. de Jesus at al. 2011, Correira et al 2017). Holes for rivets or screw connections in steel plates are prepared according to the recommendations of e.g. Eurocode 3 (2006), Simones da Silva et al. (2010). The bolts or screws are subjected to shear

* Corresponding author. Tel.: +420 532 290 361;
E-mail address: seitl@ipm.cz

2452-3216
Peer-review under responsibility of the Scientific Committee of ICSI 2017
10.1016/j.prostr.2017.07.046

or tension loading and it is supposed that they are weak points of joints. Nevertheless, in each structural element of a bridge, inhomogeneity, intrusion or scratch etc. can be assumed. A fatigue crack could start from these general stress concentrators . The detection of cracks depends on the used equipment, but usually the detectable crack length is from 1 up to 5 mm, see e.g. Dexter & Ocel (2013). The prediction of fatigue crack propagation and the estimation of remaining serviceable life can be implemented to e.g. software FCProbCalc (Fatigue Crack Probability Calculation) Krejsa et al. (2016a, 2016b, 2017a, 2017b) or sensitivity analysis Kala (2008), Kala & Valeš (2017) etc.

In this paper, calibration curves for short edge cracks that grow near a hole are proposed for several load regimes, see Fig. 1. They are the normal tension load and three cases of a bending load: pure bending, three point bending and four point bending. Calibration curves can be used as input information for software used for a refined prediction of fatigue life. Calibration curves are mostly used for the evaluation of data from experimental measurement and the accuracy fits are usually done for the relative crack lengths a/W from 0.2 to 0.8. In this analysis, calibration curves from a numerical solution for relatively short edge cracks (a/W from 0.05 to 0.13 according to the EN 1993-1-8 Eurocode 3: 2006 and from 0.05 to 0.17 according to Correia et al. (2017)) are presented and compared with calibration curves for similar cases but without holes. . The limit values $a/W = 0.13$ and 0.17 are maximum crack lengths where the crack tips reach the hole edge.

Nomenclature

2D	two-dimensional
3PB	three point bending
4PB	four point bending
FEM	finite element method
SIF	stress intensity factor
K	stress intensity factor
W	width of the specimen
B	thickness of the specimen
a	crack length
S	span
P	load force
M	bending moment
$\mathrm{d}a/\mathrm{d}N$	crack growth per cycle
ΔK	range of stress intensity factor
C, m	material properties from Paris' law
E	Young's modulus
ν	Poisson's ratio
σ	stress applied on specimen
$\Delta\sigma$	range of stress
σ_{max}	maximal value of applied stress
σ_{min}	minimal value of applied stress

2. Theoretical background

Paris-Erdogan's law

In order to describe the propagation of a crack, linear elastic fracture mechanics (Anderson 1991, Klesnil & Lukáš 1992, Suresh 1998) is typically applied. This method uses Paris-Erdogan's law (Paris & Erdogan 1963) and defines the relation between the propagation rate of the crack size a, and the range of the stress rate coefficient, ΔK, in the face of the crack:

$$\frac{da}{dN} = C(\Delta K)^m, \tag{1}$$

where C and m are material constants for a particular material and environment (temperature, humidity, etc..), N is the number of loading cycles and ΔK is the range of the stress intensity factor in front of the crack tip and it is defined as follows:

$$\Delta K = \Delta\sigma\sqrt{\pi a} f(a/W), \tag{2}$$

where $\Delta\sigma$ is the constant stress range (the value of $\Delta\sigma = \sigma_{max}$-$\sigma_{min}$ corresponding to each way of loading is shown in Table 1.), a is the crack length and $f(a/W)$ is the calibration curve which represents various boundary conditions.

The value of fracture toughness can be determined by substituting the critical loading σ_C (when crack growth starts) in place of $\Delta\sigma$ in eq (2) and setting ΔK to K_{IC}.

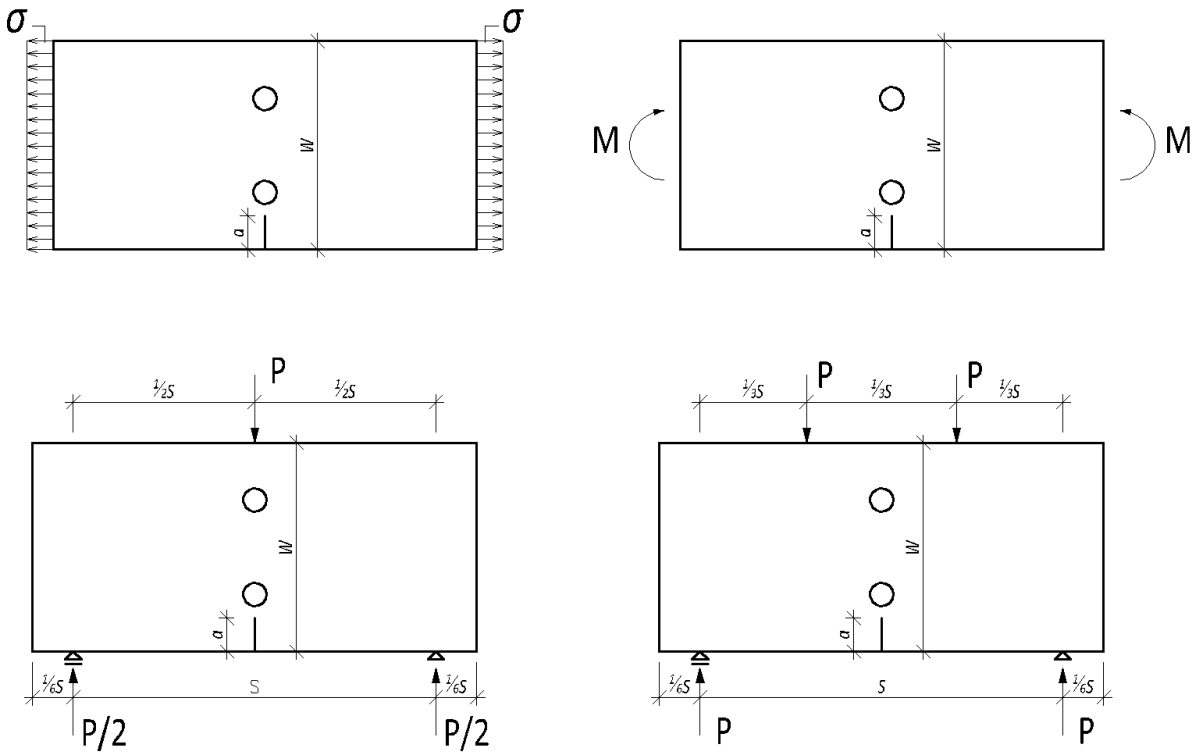

Fig. 1. Various loads used for a numerical simulation of introduced configurations: (a) tension load; (b) pure bending moment load (c) three point bending load and (d) four point bending load.

Table 1. An explanation of $\Delta\sigma$ for the various loading modes investigated.

Type of load	Tension	Pure bending	Three-point bending	Four-point bending
Stress σ	$\sigma = \frac{P}{WB}$	$\frac{6M}{W^2B}$	$\frac{3PS}{2W^2B}$	$\frac{2PS}{W^2B}$

The calibration curves $f(a/W)$ for standard specimens or well-known configurations can be found in Handbooks proposed by Murakami (ed.) (1987), Tada et al.(2000). For the studied configurations similar ones are the single edge notch specimen and the pure bending specimen, see e.g. Tada et al. (2000):

$$f(a/W) = 1.122 - 1.40(a/W) + 7.33(a/W)^2 - 13.08(a/W)^3 + 14.0(a/W)^4. \quad (3)$$

Accuracy 0.2% for $a/W \leq 0.6$
or

$$f(a/W) = \sqrt{\frac{2W}{\pi a} tan \frac{\pi a}{2W}} \frac{0.923+0.199(1-sin\frac{\pi a}{2W})^4}{cos\frac{\pi a}{2W}}. \quad (4)$$

Accuracy better than 0.5% for any a/W.

3. Finite element model

With the geometry presented in Fig. 1, finite element (FE) models were meshed with the element type PLANE183 from the software ANSYS. The above-mentioned element is used in order to take the crack tip singularity (KSCON) into account and the stress intensity factors were calculated from displacements of nodes at the crack tip by means of the implemented procedure KCALC, see Fig. 2a detail in Fig. 2b.The FE model was modelled as a 2D model with plane strain conditions. The following step was the application of the boundary conditions, according to Tab. 1.

3.1. Material properties

The material properties of steel used as inputs for the FE analysis were Young's modulus and Poisson's ratio, E= 210 GPa and v = 0.3, respectively.

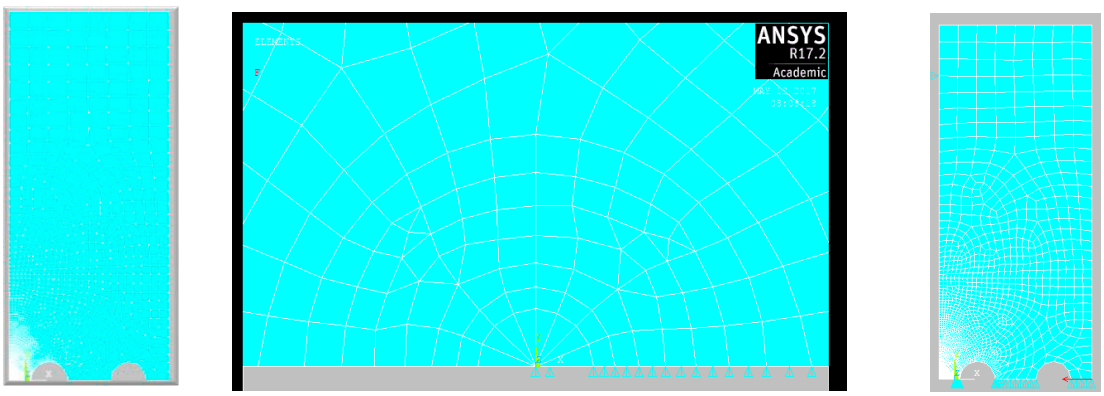

(a) (b) (c)

Fig. 2. Finite element model (a) example of pure bending with holes; (b) detail of a crack tip (KSCON) and (c) used boundary conditions.

Table 2. Reference values of $f(a/W)$ for pure and three point bending.

Type of load	Pure bending				Three-point bending		
a/W	Tada et al 2000	Guinea et al. 1998	Bakker 1995	**Present study**	Tada et al 2000	Bakker 1995	**Present study**
0.1	1.041	1.027	1.047	**1.048**	1.007	0.980	**0.981**
0.3	1.098	1.092	1.124	**1.125**	1.045	1.045	**1.041**

3.2. Accurate finite element analyses of pure bending

In this first part of the study, convergence analyses were performed in order to obtain accurate stress intensity factor values. According to Tada et al. 2000, the non-dimensional stress intensity factor (calibration curves) for an edge crack loaded by pure bending is defined in eqs. (3-4). For this configuration, a 2D model using 2800 elements was performed.

Comparisons of the results from this study and several of those extracted from the literature for pure and three point bending, are shown in Table 2. The data from this paper agree very well and could be subjected to analysis.

4. Results and discussion

4.1. Tension load

Typical geometry functions determined for a tensile load can be introduced as follows:

a) for a crack in an infinite plate it holds $f(a/W) = 1$, note that the whole fracture mechanics theory was postulated for this kind of crack configuration, e.g. Anderson (1991), Suresh (1998), Tada et al. (2000).
b) for an edge crack in a semi-infinite plate $f(a/W) = 1.12$, e.g. Murakami et al. (1987), Anderson (1991), Suresh (1998), Tada et al. (2000).
c) for an edge crack in a finite plate for the *a/W* interval from 0.01 to 0.3, (Seitl et al 2018), see Fig.3 and 4.

$$f(a/W) = 1.122 + 0.1444(a/W) + 5.3578(a/W)^2 + 0.5477(a/W)^3 \quad (5)$$

d) for an end edge crack in a finite plate with a hole (the EN 1993-1-8 Eurocode 3: 2006) for an interval from 0.01 to 0.13, see Fig. 3

$$f(a/W) = 0.9919 - 16.94(a/W) + 1095.6(a/W)^2 - 15122(a/W)^3 - 72020(a/W)^4 \quad (6)$$

e) for an end edge crack in a finite plate with a hole (Correia et al. 2017) for an interval from 0.01 to 0.17, see Fig. 4

$$f(a/W) = 1.061 - 9.83(a/W) + 461.19(a/W)^2 + 5164.5(a/W)^3 - 19667(a/W)^4 \quad (7)$$

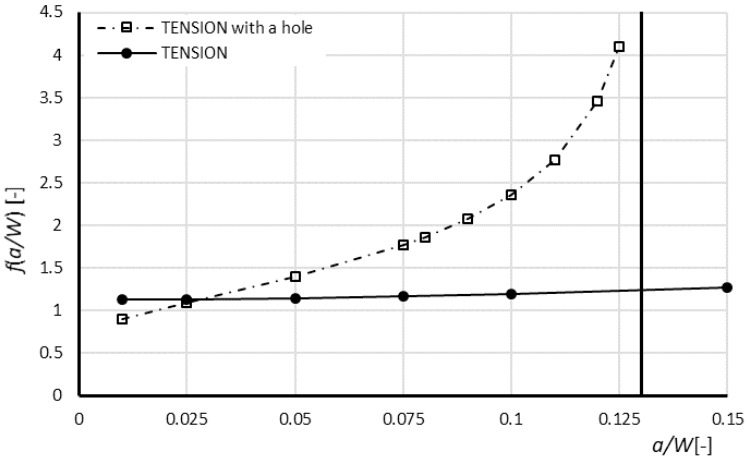

Fig. 3 Comparison of calibration curves for a short edge crack loaded by tension with and without a hole, the hole edge starts at the distance *a/W*=0.13 (the EN 1993-1-8 Eurocode 3: 2006)

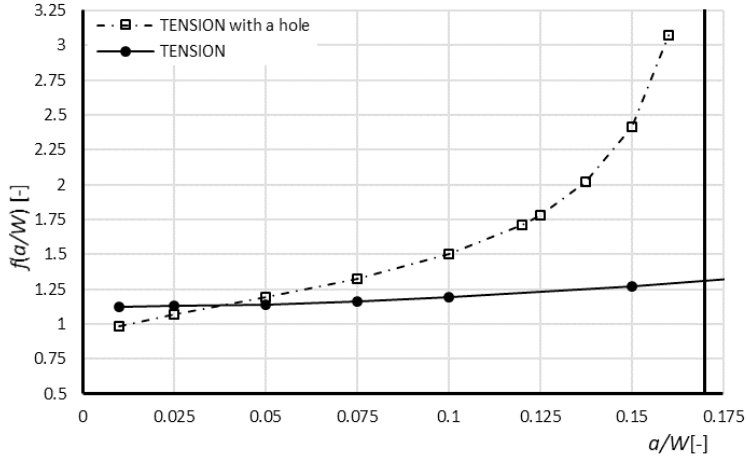

Fig. 4 Comparison of calibration curves for a short edge crack loaded by tension with and without a hole, the hole starts at the distance *a/W*=0.17 (Correia et al. 2017)

4.2. Bending load

Figs. 5 and 6 compare the obtained calibration curves from FEM for various load types: pure, three and four point bending for edge cracks propagation in a specimen with a hole and without a hole, the hole edge starts at *a/W*=0.13 and 0.17, respectively. The curves used for the plate without a hole have a lower slope than for the plate with a hole. The types of bending loads are not negligible either, that can be seen in Figs 5 and 6, where the difference increases in comparison for the plate without a hole.

The calibration curves can be given by the following polynomial functions:

for a hole edge in *a/W*=0.13

$$f(a/W)_{pure} = 1.1963 - 16.195(a/W) + 847.57(a/W)^2 - 11555(a/W)^3 + 54644(a/W)^4 \quad (8)$$

$$f(a/W)_{3PBT\ S/W=4} = 1.0622 - 14.373(a/W) + 753.35(a/W)^2 - 10274(a/W)^3 + 48598(a/W)^4 \quad (9)$$

$$f(a/W)_{3PBT\ S/W=8} = 1.1293 - 15.284(a/W) + 800.45(a/W)^2 - 10914(a/W)^3 + 51620(a/W)^4 \quad (10)$$

$$f(a/W)_{4PBT\ S/W=4} = 1.2305 - 16.564(a/W) + 860.97(a/W)^2 - 11732(a/W)^3 + 55468(a/W)^4 \quad (11)$$

$$f(a/W)_{4PBT\ S/W=8} = 1.1972 - 16.208(a/W) + 848.04(a/W)^2 - 11560(a/W)^3 + 54670(a/W)^4 \quad (12)$$

for a hole at a/W=0.17

$$f(a/W)_{pure} = 1.17 - 9.6362(a/W) + 348.7(a/W)^2 - 3836.9(a/W)^3 + 14488(a/W)^4 \quad (13)$$

$$f(a/W)_{3PBT\ S/W=4} = 1.0735 - 8.7796(a/W) + 314.69(a/W)^2 - 3464.2(a/W)^3 + 13097(a/W)^4 \quad (14)$$

$$f(a/W)_{3PBT\ S/W=8} = 1.1218 - 9.1768(a/W) + 330.8(a/W)^2 - 3641.7(a/W)^3 + 13766(a/W)^4 \quad (15)$$

$$f(a/W)_{4PBT\ S/W=4} = 1.2041 - 9.8225(a/W) + 352.6(a/W)^2 - 3879.4(a/W)^3 + 14.656(a/W)^4 \quad (16)$$

$$f(a/W)_{4PBT\ S/W=8} = 1.1707 - 9.5852(a/W) + 347.27(a/W)^2 - 3823.1(a/W)^3 + 14447(a/W)^4 \quad (17)$$

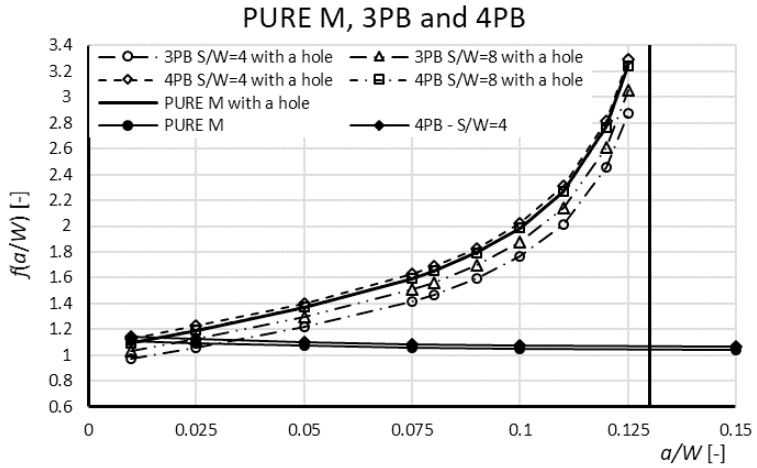

Fig. 5 Comparison of calibration curves for a short edge crack loaded by bending with and without a hole, the hole edge starts at the distance a/W=0.13 (the EN 1993-1-8 Eurocode 3: 2006)

These dependences can be important for sensitivity analysis of civil engineering steel structures under fatigue load, when calibration curves are utilized as input parameters.

5. Conclusions

A parametric study of the influence of various loads on the values of calibration functions was performed for an edge crack in a plate with holes. The following conclusions can be drawn from the results obtained:

The influence of riveted or screw holes is dominant for the values of calibration curves. The types of bending loads are not negligible, that could be seen in Figs 5and 6.

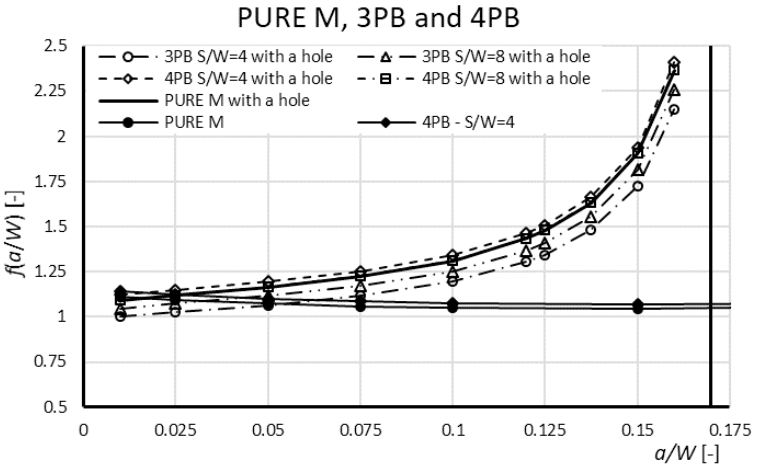

Fig. 6 Comparison of calibration curves for a short edge crack loaded by bending with and without a hole, the hole edge starts at the distance a/W=0.17 (Correia et al. 2017)

Acknowledgements

The authors acknowledge the support of the Czech Sciences foundation project No.17-01589S.

References

Anderson, T.L., 1991 Fracture Mechanics: Fundamentals and Applications, Taylor & Francis Group 1991.

ANSYS, www.ansys.com

Bakker, A.D. 1995, International Journal of Fracture 71, p323–343

Correia, J.A.F.O., Pedrosa, B., Raposo, P., De Jesus, A.M.P., Gervásio, H., Rebelo, C., Calcada, R.A.B., Simoes da Silva, L., 2017 Fatigue strength evaluation of resin-injected bolts connections using statistical analysis, Engineering, 2017 (in press)

De Jesus A.M.P., da Silva, A.L.L. Figueiredo, M.V., Correia, J.A.F.O., Ribeiro, A.S., Fernandes, A.A., 2011 Strain-life and crack propagation fatigue data from several Portuguese old metallic riveted bridges, Engineering Failure Analysis, vol. 18, pp. 148–163

Dexter, R.J. Ocel, J.M. 2013, Manual for Repair and Retrofit of Fatigue Cracks in Steel Bridges, Report: FHWA-IF-13-020, Federal Highway Administration (FHWA), Minnesota.

EN 1993-1-8 Eurocode 3: 2006 Design of steel structures - Part 1-8: Design of joints. 2006.

Guinea, G.V., Pastor, J.Y., Planas, J., Elice, M., International Journal of Fracture, 89, p. 103–

Kala, Z., Valeš, J., 2017. Global sensitivity analysis of lateral-torsional buckling resistance based on finite element simulations. Engineering Structures 134, 37–47.

Kala, Z., 2008. Fuzzy probability analysis of the fatigue resistance of steel structural members under bending. Journal of Civil Engineering and Management 14(1), 67–72.

Klesnil, M., Lukáš, P., 1992 Fatigue of metallic materials, Elsevier,

Krejsa, M., Janas, P., Krejsa, V., Kala, Z., Seitl, S. 2016a DOProC-based reliability assessment of steel structures exposed to fatigue, Perspectives in Science, vol. 7, pp. 228–235.

Krejsa, M., Seitl, S., Brozovsky, J., Lehner, P., 2017a, Fatigue damage prediction of short edge crack under various load: Direct Optimized Probabilistic Calculation, Structural Integrity Procedia (in press)

Krejsa, M., Kala, Z., Seitl, S. 2016b Inspection Based Probabilistic Modeling of Fatigue Crack Progression Procedia Engineering, vol. 142, pp. 146–153.

Krejsa, M., Koubová, L., Flodr, J., Protivinský, J., Nguyen, Q.T., 2017b Probabilistic prediction of fatigue damage based on linear fracture mechanics Frattura ed Integritta Strutturale, 11 (39), p. 143–159

Murakami, Y. (ed.) 1987 Stress Intensity Factors Handbook. In 2 Volumes. Oxford etc., Pergamon press, XLIX, XXXIX, pp. 1456.

Paris P., Erdogan, F., 1963 A critical analysis of crack propagation laws, Journal of Basic Engineering, vol. 85(4), pp. 528–533

Schijve, J., 2003 Fatigue of structures and materials in the 20th century and the state of the art, International Journal of Fatigue, vol. 25, pp. 679–702

Seitl, S., Miarka, P., Malíková, L., Krejsa, M. 2018 Comparison of calibration functions for short edge cracks under selected loads, Key Engineering Materials, vol. pp. (in press)

Simoes da Silva, L., Simoes, R., Gervásio, H., 2010 Design of Steel Structures, ECCS | Ernst & Sohn pp.454.

Suresh, S., 1998 Fatigue of materials, 2nd ed. Cambridge: Cambridge University Press.

Tada H, Paris P, Irwin G. 2000 The stress analysis of cracks handbook, 3rd ed. New York, London: ASME Press Professional Engineering Publishing; XX, p.677.